Breast Cancer Research

RESEARCH

Open Access

Preclinical evaluation of ^{64}Cu-labeled cetuximab in immuno-PET for detecting sentinel lymph node metastasis in epidermal growth factor receptor-positive breast cancer

Takeshi Usui[1], Tomohiro Miyake[1*], Tadashi Watabe[2,3], Hiroki Kato[4], Yukie Yoshii[5], Sadahiro Naka[6], Kaori Abe[1], Misato Masuyama[1], Nanae Masunaga[1], Tetsuhiro Yoshinami[1], Masami Tsukabe[1], Yoshiaki Sota[1], Tomonori Tanei[1], Masafumi Shimoda[1] and Kenzo Shimazu[1]

Abstract

Background Despite advances in breast cancer imaging, reliable detection of sentinel lymph node (SLN) metastasis remains challenging. This study aimed to determine the ability of immuno-positron emission tomography (PET) using ^{64}Cu-labeled cetuximab to detect SLN metastasis in a model of epidermal growth factor receptor (EGFR)-positive breast cancer.

Methods The SLN metastasis model was established using the EGFR-strongly-expressing MDA-MB-468 breast cancer cell line. In this xenograft model, [^{64}Cu]Cu-PCTA-cetuximab was administered intravenously (5.8 ± 0.9 MBq; $n = 12$) or both intradermally and subdermally into the parapapillary region of the tumor-containing mammary gland (4.3 ± 0.4 MBq; $n = 11$), after which PET was performed. ^{18}F-FDG PET was also performed intravenously (9.1 ± 1.4 MBq; $n = 4$) or intradermally/subdermally (5.4 ± 2.2 MBq; $n = 3$) in the same cohort before [^{64}Cu]Cu-PCTA-cetuximab PET. PET/computed tomography was performed 60 min after administration of ^{18}F-FDG and 24 h after administration of [^{64}Cu]Cu-PCTA-cetuximab. Delayed PET/CT scans were conducted 48 h after administration for all mice in the intradermally/subdermally administered [^{64}Cu]Cu-PCTA-cetuximab group and for four of the 12 mice in the intravenously administered [^{64}Cu]Cu-PCTA-cetuximab group. SLNs were identified using blue dye, and PET and pathological evaluations of the resected SLN were performed to confirm metastases.

Results After intravenous administration of [^{64}Cu]Cu-PCTA-cetuximab ($n = 12$), accumulation was detected in the primary tumor in all mice and in the axilla of eight mice (67%, SUV_{max} 1.24 ± 0.51), all of which were found to have SLNs with histologically confirmed metastasis. The sensitivity, specificity, accuracy, and negative and positive predictive values for PET with intravenously administered [^{64}Cu]Cu-PCTA-cetuximab were 89%, 100%, 92%, 75%, and 100%, respectively. In contrast, all mice with intradermal/subdermal administration ($n = 11$) showed high accumulation in both the primary tumor and axillary lymph nodes (SUV_{max} 4.28 ± 1.19), with six mice (55%, SUV_{max}

*Correspondence:
Tomohiro Miyake
t_miyake@onsurg.med.osaka-u.ac.jp

Full list of author information is available at the end of the article

5.01 ± 1.12) having histologically confirmed metastasis. The sensitivity, specificity, accuracy, and positive predictive values for PET with intradermally/subdermally administered [^{64}Cu]Cu-PCTA-cetuximab were 100%, 0%, 55% and 55%, respectively. SLN metastasis was not detectable by intravenous or intradermal/subdermal ^{18}F-FDG PET.

Conclusions PET with intravenously administered [^{64}Cu]Cu-PCTA-cetuximab demonstrated high precision for diagnosis of SLN metastasis in a xenograft model of EGFR-positive human breast cancer. Although further evaluation is necessary, intradermal/subdermal administration could be a useful therapeutic approach owing to its high accumulation in SLNs.

Keywords Immuno-PET, Sentinel lymph node metastasis, Epidermal growth factor receptor, Breast cancer

Background

Axillary lymph node metastasis is a significant prognostic factor in breast cancer, and its detection is important when determining adjuvant treatment strategies. In the past, axillary lymph node dissection has been performed for axillary staging and regional control. Nowadays, sentinel lymph node (SLN) biopsy is considered a less invasive axillary staging method for clinically node-negative (cN0) breast cancer [1]. Nevertheless, SLN biopsy is associated with complications, including shoulder abduction deficit (13.2%), arm volume difference (16.7%), arm numbness (7.5%), and tingling (6.7%) [2]. Therefore, a less invasive axillary staging method is needed.

Recent studies have explored various non-invasive methods for axillary staging, including ultrasound, computed tomography (CT), magnetic resonance imaging, and positron emission tomography (PET). The respective sensitivity and specificity of these methods have varied from 49 to 87% and 56–97% for ultrasound, 40–100% and 44–100% for magnetic resonance imaging, 60–80% and 76–97% for CT, and 20–89% and 77–100% for ^{18}F -fluorodeoxyglucose (FDG) PET [3–5]. Given the low false-negative rate of SLN biopsy (7.3–10%) [6], these imaging techniques cannot replace SLN biopsy in current practice.

Immuno-PET has emerged as a cutting-edge molecular imaging method that leverages radiolabeled antibodies for precise detection and quantification of cancer-specific molecular markers with notable sensitivity and specificity [7]. Beyond its diagnostic ability, immuno-PET shows potential as a therapeutic modality by utilizing anticancer antibodies, and thus it is a promising candidate for theranostic (therapeutic and diagnostic) applications. Research has focused primarily on its ability to identify human epidermal growth factor receptor 2 (HER2)-positive breast cancer, which accounts for about 20% of cases, by use of radiolabeled trastuzumab, a therapeutic anti-HER2 monoclonal antibody. Findings indicate that immuno-PET using ^{89}Zr-labeled or ^{64}Cu-labeled trastuzumab has high sensitivity for detection of brain metastases in patients with HER2-positive breast cancer, although its therapeutic impact is not fully clear [8, 9]. On the other hand, in estrogen receptor (ER)-positive breast cancer, which accounts for more than 70% of all cases, ligand-based PET imaging using 16α-[^{18}F]-fluoro-17β-estradiol ([^{18}F]-FES), a radiolabeled form of estradiol, has demonstrated high diagnostic accuracy in detecting ER-positive metastases and mapping functional ER distribution [10, 11]. Notably, this technique is not classified as immuno-PET, as it targets the hormone receptor through a ligand-based mechanism rather than using radiolabeled antibodies. In contrast, no studies to date have investigated immuno-PET for triple-negative breast cancer, defined by the absence of hormone receptor and HER2 expression.

Our research has concentrated on the epidermal growth factor receptor (EGFR), which is present in about 15% of breast cancers and in 50% of triple-negative cases [12]. EGFR overexpression is common in a number of cancers, and cetuximab, an anti-EGFR antibody, has shown effectiveness in colorectal [13], head and neck [14], non-small cell lung [15] cancers, as well as some potential in metastatic triple-negative breast cancer [16]. When tagged with radioisotopes, cetuximab emerges as a viable option for theranostic application. Specifically, ^{64}Cu, owing to its β^+ and β^- decay and electron capture properties and its relatively long half-life (12.7 h), is an ideal radionuclide for theranostics, facilitating both PET imaging and internal radiotherapy [17]. The efficacy of ^{64}Cu-labeled cetuximab in detection of disseminated EGFR-positive gastrointestinal cancer and its antitumor capability has been demonstrated in a preclinical model [18]. Therefore, ^{64}Cu-labeled cetuximab may have diagnostic and therapeutic potential for EGFR-positive breast cancer, potentially obviating the need for SLN biopsy in clinically node-negative (cN0) disease and axillary lymph node dissection even when SLN metastasis is present.

This study aimed to determine the diagnostic value of immuno-PET using ^{64}Cu-labeled cetuximab in a model of breast cancer with strong EGFR expression and SLN metastasis by comparing the efficacy of intravenous (IV) versus intradermal/subdermal (ID/SD) administration, noting that the latter method is conventionally used to identify SLNs in clinical practice. This research will serve as the first step towards clinical application of

^{64}Cu-labeled cetuximab PET as a theranostic approach in patients with cN0 EGFR-positive breast cancer.

Materials and methods

Synthesis of [^{64}Cu]Cu-PCTA-cetuximab

[^{64}Cu]Cu-PCTA-cetuximab was prepared as described previously [18]. In brief, p-SCN-Bn-PCTA (Macrocyclics) was dissolved in dimethyl sulfoxide and added to 2 mg/mL cetuximab (ERBITUX, Merck) in 50 mM boric acid buffer (pH 8.5) at a chelate to antibody molar ratio of 5:1. The reaction was performed at 37 °C for approximately 24 h with shaking. Next, PCTA-cetuximab, solvent-exchanged and adjusted to a concentration of 0.2 mg/mL with 0.1 M acetate buffer (pH 6.0), was used for radiolabeling.

[^{64}Cu]$CuCl_2$ (74–111 MBq) sourced from PDRadiopharma was solvent-exchanged with 0.1 M acetate buffer (pH 6.0). Next, 600 µL of 0.2 mg/mL PCTA-cetuximab (120 µg) were added to 486 µL of [^{64}Cu]$CuCl_2$ solution (approximately 60 MBq). The labeling reaction was performed at 40 °C for 60 min to obtain [^{64}Cu]Cu-PCTA-cetuximab with a radiochemical purity of > 90%.

Preparation of xenograft models

The MDA-MB-468 triple-negative breast cancer cell line, characterized by a lack of the estrogen receptor, progesterone receptor, and HER2 expression while exhibiting strong positivity for EGFR, was used in this study. The MDA-MB-468 cells were obtained from the American Type Culture Collection and cultured in Dulbecco's Modified Eagle Medium supplemented with L-glutamine and phenol red (Sigma-Aldrich) and with 10% heat-inactivated fetal bovine serum (FB-1290, Biosera). Tumor xenograft models were established by subcutaneous injection of 5×10^6 MDA-MB-468 cells suspended in phosphate-buffered saline (0.05 mL) and Matrigel (1:1; BD Biosciences) into the left third mammary gland of female non-obese diabetic (NOD)/severe combined immunodeficiency (SCID) mice purchased from CLEA Japan, Inc. The mice were assessed 3 weeks post-implantation when the tumor had reached approximately 0.5–1 cm in diameter. The mice were euthanized under deep anesthesia with isoflurane inhalation when signs of intolerable distress or weight loss of > 20% was observed.

[^{64}Cu]Cu-PCTA-cetuximab and ^{18}F-FDG PET imaging and analysis

To determine the most effective [^{64}Cu]Cu-PCTA-cetuximab delivery method for detection of SLN metastasis, we compared PET probe administration via two different routes, IV and ID/SD, using MDA-MB-468 xenograft mice and negative control mice. In the IV group, 12 xenograft mice (aged 11 weeks, weight 19.2 ± 0.9 g) and one negative control mouse (age 11 weeks, weight 17.2 g) received [^{64}Cu]Cu-PCTA-cetuximab (5.8 ± 0.9 MBq; around 10.6 ± 1.3 µg of mouse anti-EGFR antibody; total volume 50–100 µL) via the tail vein, followed by PET/CT imaging (Fig. 1). Four of the 12 xenograft mice were also

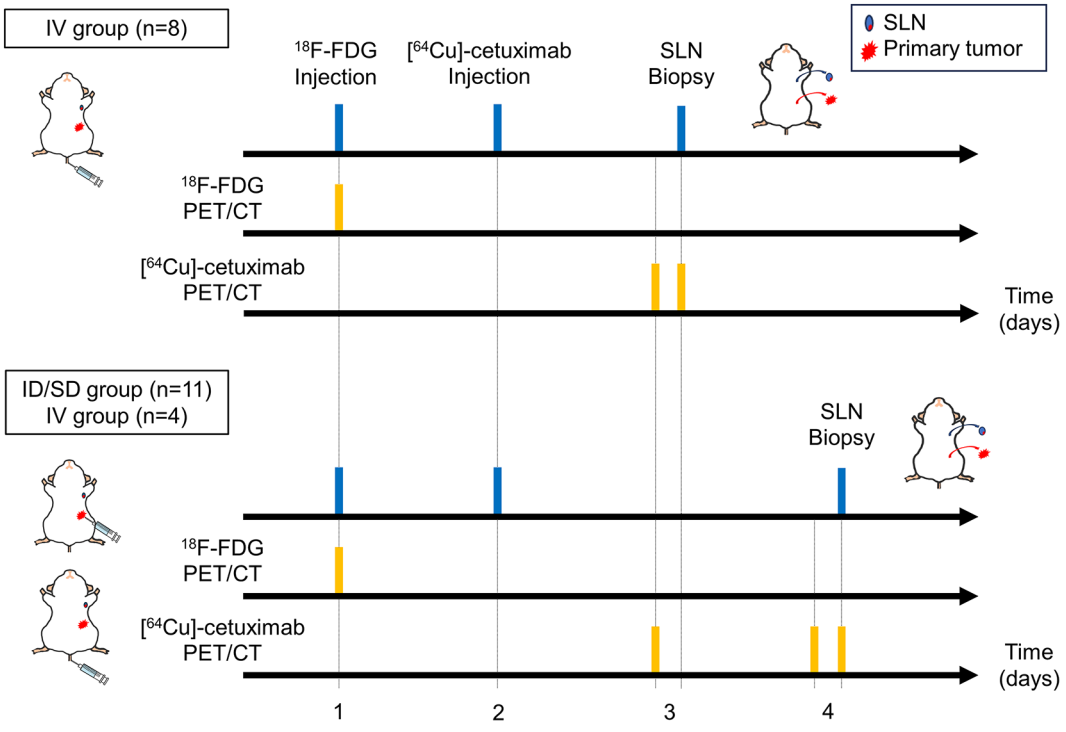

Fig. 1 Summary of the study protocol for administration of radiotracers and PET/CT imaging

evaluated by ^{18}F-FDG PET (9.1 ± 1.4 MBq; total volume 50–100 µL, administered IV) one day before administration of [^{64}Cu]Cu-PCTA-cetuximab. In the ID/SD group, 11 xenograft mice (age 11 weeks, weight 20.5 ± 1.2 g) and a negative control mouse (age 11 weeks, weight 18.0 g) received [^{64}Cu]Cu-PCTA-cetuximab (4.3 ± 0.4 MBq; approximately 9.6 ± 0.9 µg of mouse anti-EGFR antibody; total volume 50–100 µL) administered to the parapapillary region of the mammary gland containing the primary tumor. Of these, three xenograft mice were also evaluated by ^{18}F-FDG PET (5.4 ± 2.2 MBq; total volume 50–100 µL).

PET/CT scans were performed under isoflurane anesthesia using an Inveon PET/CT scanner (Siemens Healthcare) 60 min after administration of ^{18}F-FDG and 24 h after administration of [^{64}Cu]Cu-PCTA-cetuximab. Delayed PET/CT scans were conducted 48 h post-administration for all mice in the ID/SD [^{64}Cu]Cu-PCTA-cetuximab group, as well as for four of the 12 mice in the IV [^{64}Cu]Cu-PCTA-cetuximab group, due to an identical experimental timeline. After final PET/CT scanning, SLN biopsies were performed under isoflurane anesthesia. The mice and the excised SLNs were then imaged by PET/CT, which identified the SLN by PET positivity and disappearance of axillary accumulation in the post-SLN biopsy on PET.

The PET data were reconstructed using three-dimensional ordered-subset expectation maximization (16 subsets, two iterations), followed by maximum a posteriori estimation with scatter and attenuation correction. Radioactivity uptake was decay-corrected to the injection time and expressed as the standardized uptake value (SUV). Ellipsoid regions of interest were placed manually on the SLNs, tumors, heart, liver, spleen, and muscle using AMIDE (Ver. 1.0.6) [19]. PET accumulation was considered positive when the signal intensity exceeded that of the surrounding muscle or soft tissue by more than two standard deviations.

SLN biopsy in xenograft models

The SLN biopsy was performed using blue dye (Fig. 2a). Specifically, 40 µL of patent blue were injected both ID and SD into the parapapillary region of the left third mammary gland. After confirming that the lymphatic vessels stained blue from the body surface, the abdominal skin was incised in the midline. The subcutis was then peeled off, and the blue-stained axillary lymph node was sampled. The mice were observed and SLN biopsies were performed under deep anesthesia with isoflurane.

Immunohistochemistry of SLN

After the animals were euthanized, the tumor xenografts and SLNs were resected and fixed with 10% paraformaldehyde overnight at room temperature. The fixed tissues were paraffin-embedded, and 4-µm-thick sections that were spaced at 100 µm intervals were prepared. Immunohistochemical staining was performed to confirm SLN metastasis in xenografts using an anti-pan cytokeratin (CK) antibody (AE1AE3; Nichirei Biosciences) and an anti-EGFR antibody (clone D38B1; Cell Signaling Technology) at a dilution of 1:50 in dilution buffer according to the manufacturer's protocols.

For anti-CK staining, antigen retrieval was performed at 98 °C in pH 9 solution (S2367; Agilent) for 20 min in a water bath. For EGFR staining, antigen retrieval was performed at 98 °C in pH 8 (#14747; Cell Signaling Technology) solution for 15 min in a microwave. The stained slides were imaged at 40× and 200× magnification using BZ-9000 (Keyence) and ECLIPSE Ci (Nikon) microscopes. Representative results are shown in Fig. 2b.

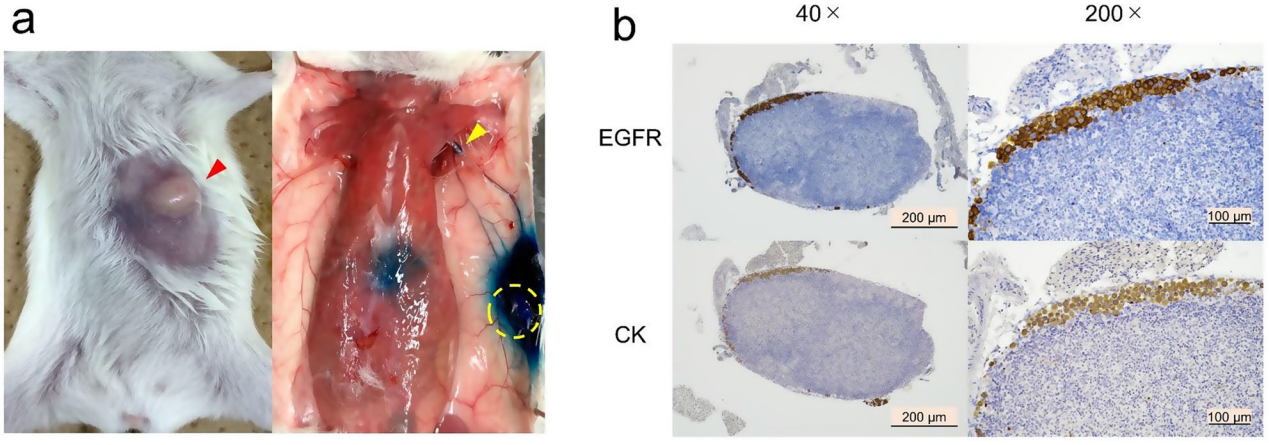

Fig. 2 MDA-MB-468 xenograft model with SLN metastasis. (**a**). MDA-MB-468 xenograft model with the primary tumor in the third left mammary gland (red arrow and yellow dotted circle). SLN is detected by SLN mapping using patent blue (yellow arrow). (**b**). SLN metastasis detected by EGFR and CK immunohistochemistry (left, low magnification [×40]; right, high magnification [×200])

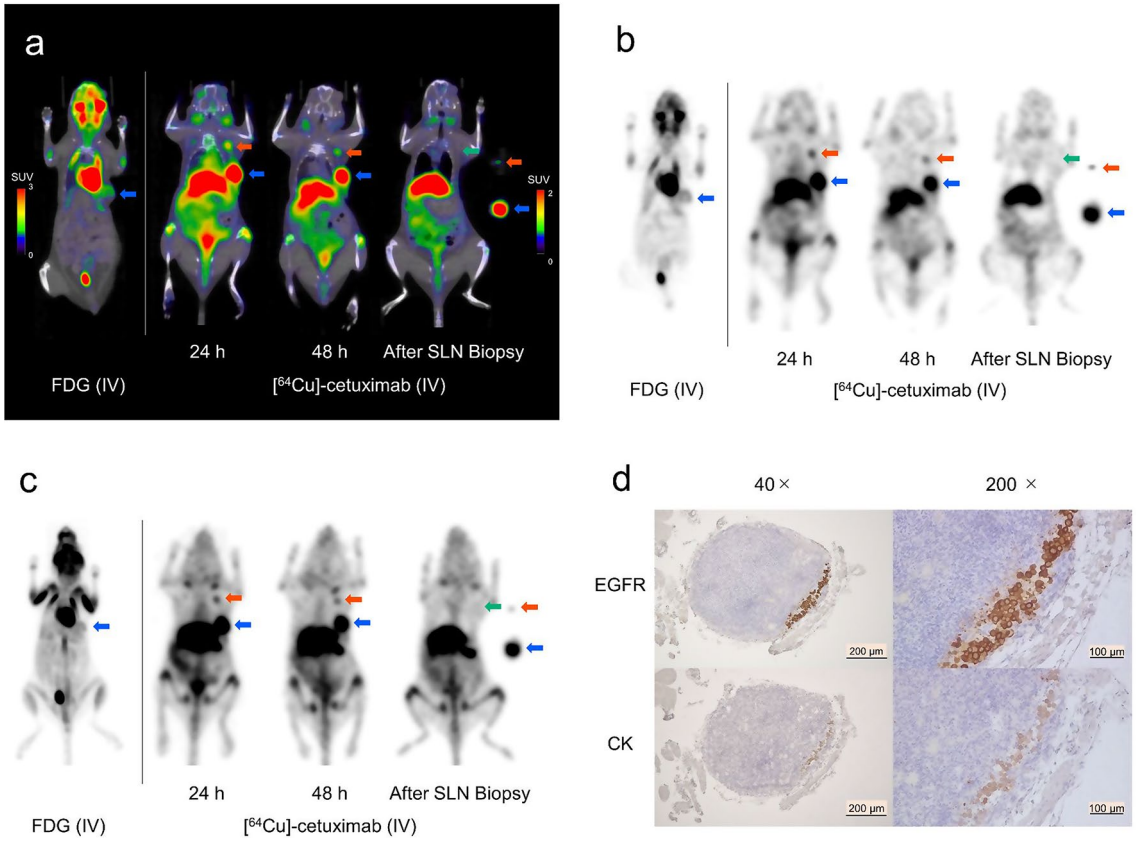

Fig. 3 PET/CT images and immunostaining of SLN metastasis in MDA-MB-468 xenograft after IV [^{64}Cu]Cu-PCTA-cetuximab. Representative (**a**). coronal PET/CT, (**b**). coronal PET and (**c**). MIP images in an MDA-MB-468 xenograft with SLN metastasis at 60 min after IV ^{18}F-FDG injection, 24 h and 48 h after IV [^{64}Cu]Cu-PCTA-cetuximab injection, and following SLN biopsy. Red arrows indicate metastatic SLN and the green arrow denotes disappearance of the lymph node with accumulation of [^{64}Cu]Cu-PCTA-cetuximab. The blue arrow denotes the primary tumor. (**d**). EGFR and CK immunostaining of the SLN in the MDA-MB-468 xenograft (left, low magnification [×40]; right, high magnification [×200])

Statistics

Continuous variables were compared between groups using the *t*-test in EZR* (version 4.3.1) [20]. A p-value < 0.05 was considered statistically significant.

Results

Detection of SLN metastasis by IV [^{64}Cu]Cu-PCTA-cetuximab PET

Figure 3a, b and c show representative PET images following IV administration of [^{64}Cu]Cu-PCTA-cetuximab in an MDA-MB-468 xenograft mouse model with SLN metastasis. Notably, IV [^{64}Cu]Cu-PCTA-cetuximab PET demonstrated significant accumulation in the primary tumor (diameter 7 mm) located in the left third mammary gland (SUV_{max} 4.95) and left axillary lymph nodes (SUV_{max} 2.32). Subsequent to an SLN biopsy, we observed both the presence of [^{64}Cu]Cu-PCTA-cetuximab uptake in the excised SLN and absence of [^{64}Cu]Cu-PCTA-cetuximab uptake in the resected axillary lymph node area, confirming accurate identification of the metastatic SLN. Immunohistochemical analyses with anti-CK and anti-EGFR staining revealed a metastatic lesion measuring 0.5 mm within the SLN (Fig. 3d).

Table 1 Comparison of PET/CT detection of SLN metastasis using IV [^{64}Cu]Cu-PCTA-cetuximab and IV ^{18}F-FDG

PET/CT	Pathology	
	Positive	Negative
IV [^{64}Cu]Cu-PCTA-cetuximab PET/CT		
Positive	8	0
Negative	1	3
IV ^{18}F-FDG PET/CT		
Positive	0	0
Negative	4	0

Table 1 summarizes the diagnostic performance of IV [^{64}Cu]Cu-PCTA-cetuximab PET and IV ^{18}F-FDG PET for detection of SLN metastasis. Eight (67%) of the 12 mice evaluated showed accumulation of [^{64}Cu]Cu-PCTA-cetuximab in the axillary nodes (mean SUV_{max} 1.24 ± 0.51); all were histologically confirmed to be metastatic SLNs. The median size of these metastatic lesions was 0.4 mm (range 0.1–1.0). One of the mice in the subset without accumulation of [^{64}Cu]Cu-PCTA-cetuximab

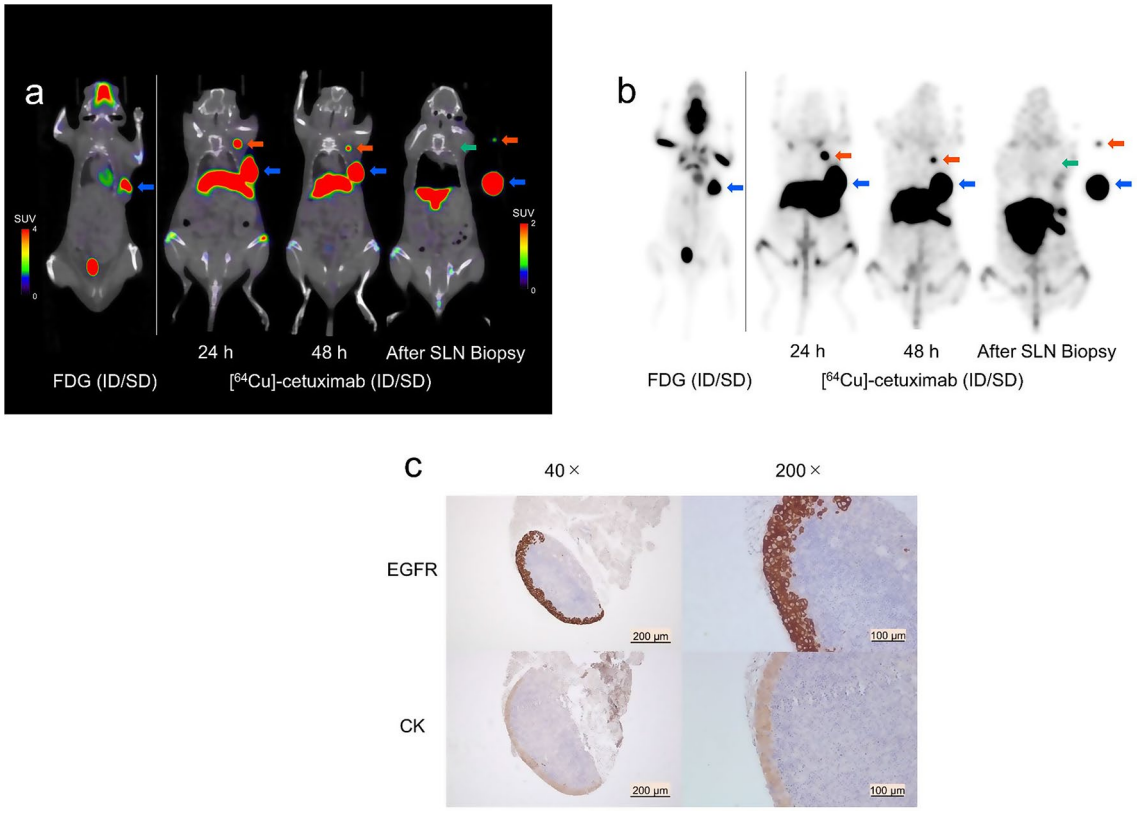

Fig. 4 PET/CT images and immunostaining of SLN metastasis in MDA-MB-468 xenograft after ID/SD [^{64}Cu]Cu-PCTA-cetuximab. Representative (**a**). PET/CT and (**b**). MIP images in an MDA-MB-468 xenograft with SLN metastasis at 60 min after ID/SD administration of ^{18}F-FDG, at 24 and 48 h after ID/SD injection of [^{64}Cu]Cu-PCTA-cetuximab, and following SLN biopsy. Red arrows indicate metastatic SLN and the green arrow denotes disappearance of the lymph node with accumulation of [^{64}Cu]Cu-PCTA-cetuximab. The blue arrow denotes the primary tumor. (**c**). EGFR and CK immunostaining of an SLN in an MDA-MB-468 xenograft after SLN biopsy (left, low magnification [×40]; right, high magnification [×200])

had histologically confirmed SLN metastasis with a lesion size of 0.4 mm. The diagnostic metrics of sensitivity, specificity, accuracy, negative predictive value (NPV), and positive predictive value (PPV) were calculated to be 89% (8/9), 100% (3/3), 92% (11/12), 75% (3/4), and 100% (8/8), respectively.

In a further experiment in which both ^{18}F-FDG and [^{64}Cu]Cu-PCTA-cetuximab were administered IV to four mice, there was no significant accumulation of ^{18}F-FDG. Conversely, accumulation of [^{64}Cu]Cu-PCTA-cetuximab was observed in the axillary nodes, which were pathologically confirmed as metastatic SLNs. On the other hand, the accumulation of ^{18}F-FDG in the brain (mean SUVmax 3.68 ± 0.34) and tumor (mean SUVmax 2.33 ± 0.26) was observed in all mice.

Detection of SLN metastasis on ID/SD [^{64}Cu]Cu-PCTA-cetuximab PET

Figure 4a and b show PET images obtained following ID/SD delivery of [^{64}Cu]Cu-PCTA-cetuximab. In the MDA-MB-468 xenograft model of SLN metastasis, high uptake of [^{64}Cu]Cu-PCTA-cetuximab was noted in both the primary tumor (SUV_{max} 11.08, 6 mm in diameter) of the left third mammary gland and the adjacent left axillary lymph nodes (SUV_{max} 5.09). Post-SLN biopsy analyses confirmed that [^{64}Cu]Cu-PCTA-cetuximab was present in the excised SLN and absent in the axillary region, which identified the excised node as the true SLN. Histology and immunohistochemistry (anti-CK and anti-EGFR) revealed a 1.1 mm metastatic focus within the SLN (Fig. 4c).

Table 2 Comparison of PET/CT detection of SLN metastasis using ID/SD [^{64}Cu]Cu-PCTA-cetuximab and ID/SD ^{18}F-FDG

	Pathology	
	Positive	**Negative**
ID/SD [^{64}Cu]Cu-PCTA-cetuximab PET/CT		
Positive	6	5
Negative	0	0
ID/SD ^{18}F-FDG PET/CT		
Positive	0	0
Negative	2	1

The ability of [^{64}Cu]Cu-PCTA-cetuximab (ID/SD) PET/CT and ^{18}F-FDG (ID/SD) PET/CT to detection SLN metastasis when administered via the intradermal lymphatic route is summarized in Table 2. All 11 mice

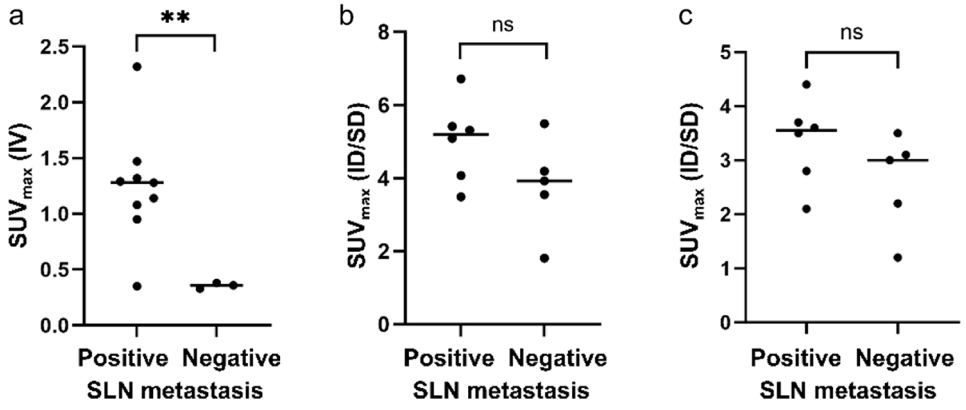

Fig. 5 Quantitative analysis of SLN uptake of [^{64}Cu]Cu-PCTA-cetuximab PET with or without pathologically confirmed SLN metastasis. Comparisons of uptake at (**a**). 24 h after IV [^{64}Cu]Cu-PCTA-cetuximab PET (**$p = 0.016$), (**b**). 24 h after ID/SD [^{64}Cu]Cu-PCTA-cetuximab PET ($p = 0.132$), and (**c**). 48 h after ID/SD [^{64}Cu]Cu-PCTA-cetuximab PET ($p = 0.179$). Black bars indicate the mean SUV$_{max}$

studied had PET-positive axillary nodes (mean SUV$_{max}$ 4.28 ± 1.19), which were confirmed as SLNs. Six (55%) of the 11 mice had histologically confirmed metastases in PET-positive SLNs (mean SUV$_{max}$ 5.01 ± 1.12), with a median size of 0.6 mm (range 0.1–1.1). This modality demonstrated sensitivity, specificity, accuracy, and a positive predictive value of 100% (6/6), 0% (0/5), 55% (6/11), and 55% (6/11), respectively.

In three of the 11 mice, [^{64}Cu]Cu-PCTA-cetuximab (ID/SD) PET/CT identified hotspots not visible on ^{18}F-FDG (ID/SD) PET/CT, 67% of which were pathologically confirmed to show axillary node involvement. On [^{64}Cu]Cu-PCTA-cetuximab (ID/SD) PET (mean 24-h SUV$_{max}$ 2.02 ± 0.74; mean 48-h SUV$_{max}$ 1.32 ± 0.79), four (36%) of these mice showed uptake in the contralateral axillary lymph nodes, which were confirmed to be SLNs by patent blue mapping (Supplementary Fig. S1a–1c). These contralateral SLNs were all pathologically negative for metastasis (Supplementary Fig. S1d).

Comparison of [^{64}Cu]Cu-PCTA-cetuximab uptake in SLNs

Figure 5 shows a quantitative comparison of PET SUV$_{max}$ in the axillary lymph nodes, examining the effects of [^{64}Cu]Cu-PCTA-cetuximab administered IV and ID/SD in nodes with or without pathological SLN metastases. The mean SUV$_{max}$ was significantly higher in SLNs positive for metastasis than in those without metastasis at 24 h after IV administration (1.24 ± 0.51 vs. 0.35 ± 0.02, $p = 0.016$; Fig. 5a). Although uptake tended to be higher in lymph nodes with metastasis, there were no significant differences in SUV$_{max}$ between the lymph node groups at 24 and 48 h following ID/SD administration (24 h, 5.01 ± 1.12 vs. 3.79 ± 1.32, $p = 0.132$; 48 h, 3.35 ± 0.79 vs. 2.60 ± 0.91, $p = 0.179$; Fig. 5b and c). Furthermore, the change in SUV$_{max}$ between 24 and 48 h did not differ significantly according to SLN metastasis status (1.46 ± 1.63 vs. 1.04 ± 0.90, $p = 0.616$).

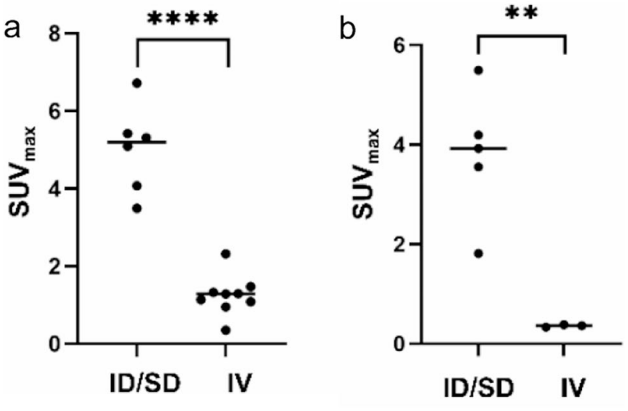

Fig. 6 [^{64}Cu]Cu-PCTA-cetuximab uptake in SLN according to whether the route of administration was IV or ID/SD. (**a**). SUV$_{max}$ in metastatic SLN at 24 h after injection of [^{64}Cu]Cu-PCTA-cetuximab (****$p < 0.001$). (**b**). SUV$_{max}$ in the non-metastatic SLN at 24 h after injection of [^{64}Cu]Cu-PCTA-cetuximab (**$p = 0.004$). Black bars indicate the mean SUV$_{max}$

We evaluated the mean SUV$_{max}$ in SLN at 24 h post-administration according to route of delivery (Fig. 6) and found that it was significantly higher in the ID/SD group than in the IV group in both the SLN metastasis-positive group and the metastasis-negative group (5.01 ± 1.12 vs. 1.24 ± 0.51, $p < 0.001$, Fig. 6a.3.79 ± 1.32 vs. 0.35 ± 0.02, $p = 0.004$, Fig. 6b). Comparison of biodistribution of [^{64}Cu]Cu-PCTA-cetuximab at 24 h after administration between the IV and ID/SD groups did not reveal any significant between-group difference in SUV$_{max}$ in the liver, spleen, heart, or muscle (Supplementary Table S1).

Discussion

This study assessed the diagnostic potential of [^{64}Cu]Cu-PCTA-cetuximab PET/CT for detection of SLN metastasis in EGFR-positive breast cancer and the effects of its route of administration in an EGFR-strongly-expressing breast cancer xenograft model.

On IV [^{64}Cu]Cu-PCTA-cetuximab PET, 67% of mice showed accumulation of radiotracer in the axillary lymph nodes, all of which were identified as SLNs and histologically confirmed to contain metastases. Notably, all the SLN metastases detected, including those in the solitary false-negative case, were no larger than 1.0 mm, indicating that they were clinically micrometastases [21], which are notoriously difficult to detect on radiological images obtained preoperatively. Despite the diminutive size of these metastatic lesions, the sensitivity, specificity, and negative predictive value of IV [^{64}Cu]Cu-PCTA-cetuximab PET was 89%, 100%, and 75%, respectively. Given the potentially enhanced accuracy of [^{64}Cu]Cu-PCTA-cetuximab PET/CT for detection of larger metastases and that the resolution of PET/CT is better in animals than in humans, further clinical research is needed to determine the value of [^{64}Cu]Cu-PCTA-cetuximab PET/CT in diagnosis of SLN metastases.

In contrast, PET/CT scans performed 24 and 48 h following ID/SD injection of [^{64}Cu]Cu-PCTA-cetuximab consistently revealed accumulation in axillary lymph nodes, identifying each as the SLN. However, pathological analysis revealed a false-positive rate of 46%. Typically, antibody agents administered via the ID/SD route are absorbed either directly into the systemic circulation or indirectly through lymphatic vessels. Given that cetuximab has a molecular weight of 145,782 Da, absorption of antibodies with a molecular weight exceeding 20 kDa occurs primarily occurs via the lymphatic vessels [22]. Therefore, we speculate that [^{64}Cu]Cu-PCTA-cetuximab, when administered ID/SD into the parapapillary region, is significantly absorbed by the lymphatic vessels, transported through the lymphatic system of the third mammary gland, and subsequently accumulates in the SLN.

In this study, we anticipated that cetuximab would selectively accumulate in metastatic lesions [23], potentially resulting in a higher SUV_{max} in metastasis-positive SLNs than in negative ones, and that the elevated SUV_{max} would be sustained over time. Unexpectedly, although the SUV_{max} tended to be higher in metastasis-positive SLNs at 24 and 48 h in the ID/SD group, this finding did not reach statistical significance. Furthermore, the rate of reduction in the amount of tracer in the SLNs between 24 and 48 h remained consistent irrespective of metastasis status. We speculated that [^{64}Cu]Cu-PCTA-cetuximab, when non-specifically trapped in the SLN could specifically re-accumulate in SLN metastases after entering the systemic circulation, but our findings did not support this theory. It is possible that the tracer injected subcutaneously into the third mammary gland remained at the injection site, resulting in sustained flow into the lymphatic vessels and subsequent accumulation in the SLN. This non-specific accumulation could potentially obscure cancer-specific binding within the SLN. Employing autoradiography could enable a more detailed analysis of the specificity of tracer uptake via the ID/SD route. Our research demonstrated that ID/SD injection of [^{64}Cu]Cu-PCTA-cetuximab leads to non-specific accumulation of tracer in SLNs and is therefore unable to detect SLN metastasis.

The SUV_{max} in SLNs was higher after ID/SD administration of [^{64}Cu]Cu-PCTA-cetuximab than after IV administration regardless of metastasis status, indicating enhanced uptake and retention of [^{64}Cu]Cu-PCTA-cetuximab in SLNs via the ID/SD route. Although IV delivery is preferred for accurate diagnosis of SLN metastases, the ID/SD route may be beneficial for localized therapy because of its high accumulation. Further studies are needed to confirm the potential of ID/SD [^{64}Cu]Cu-PCTA-cetuximab as a treatment for SLN metastases.

In this study, we compared the ability of ^{18}F-FDG to detect SLN metastasis using PET/CT with that of [^{64}Cu]Cu-PCTA-cetuximab according to whether delivery was IV or ID/SD. We found that ^{18}F-FDG did not have sufficient ability to accumulate in SLNs, irrespective of metastasis status, possibly because of the predominance of micrometastases detected in the SLN metastases and the limited sensitivity of ^{18}F-FDG for detection of small early-stage lymph node lesions [24]. Furthermore, the molecular characteristics of ^{18}F-FDG (molecular weight, 181 Da) favor its rapid systemic absorption through blood vessels over lymphatic uptake when administered ID/SD.

This study has several limitations that warrant attention in future research. First, the sample size was small, so the findings require confirmation. Second, autoradiography is a valuable technique for confirming tissue-level tracer-specific distribution in the resected SLNs; however, this analysis was not performed in the present study. Third, further investigation is required into the efficacy of [^{64}Cu]Cu-PCTA-cetuximab as a treatment for primary breast cancer and SLN metastases, as well as non-specific accumulation in inflammatory lymph nodes and side effects, as does the optimal route of administration. Finally, only an MDA-MB-468 triple-negative breast cancer cell line with high EGFR expression was used. Therefore, the generalizability of our findings may be limited. Given that EGFR is overexpressed in approximately 15% of breast cancers [25], future research should examine the theranostic potential of [^{64}Cu]Cu-PCTA-cetuximab PET/CT in other subtypes of breast cancer with varying EGFR expression levels to broaden its applicability to a wider patient population.

Our findings, that immuno-PET using IV [^{64}Cu]Cu-PCTA-cetuximab exhibited high precision for detecting SLN metastases in a xenograft model of EGFR-positive breast cancer, demonstrate significant potential for clinical application. Considering the future clinical

development of this approach, IV [^{64}Cu]Cu-PCTA-cetuximab PET could offer a non-invasive method for axillary staging, eliminating the need for conventional invasive surgical procedures such as SLN biopsy or ALND in EGFR-positive breast cancer. Furthermore, we have initiated investigations into the therapeutic effects of [^{64}Cu]Cu-PCTA-cetuximab administered via ID/SD or IV for SLN metastases in an in vivo model of EGFR-positive breast cancer. Depending on the outcomes, [^{64}Cu]Cu-PCTA-cetuximab could potentially replace surgery and serve as a less invasive local treatment for axillary metastases in EGFR-positive breast cancer.

Conclusion

This study demonstrated that immuno-PET with IV administration of [^{64}Cu]Cu-PCTA-cetuximab is a highly precise method for detecting SLN metastases in a model of EGFR-strongly-expressing triple-negative breast cancer. Its results suggest that [^{64}Cu]Cu-PCTA-cetuximab could be a diagnostic option for axillary staging of breast cancer and have a therapeutic role when administered ID/SD in view of its high accumulation in SLNs.

Abbreviations

SLN	Sentinel lymph node
PET	Positron emission tomography
EGFR	Epidermal growth factor receptor
CT	Computed tomography
FDG	Fluoro deoxy glucose
HER2	Human epidermal growth factor receptor 2
IV	Intravenous
ID/SD	Intradermal/subdermal
NOD	Non-obese diabetic
SCID	Severe combined immunodeficiency
SUV	Standardized uptake value
CK	Pan cytokeratin
NPV	Negative predictive value
PPV	Positive predictive value
MIP	Maximum intensity projection

Supplementary Information

The online version contains supplementary material available at https://doi.org/10.1186/s13058-025-01972-4.

Supplementary Material 1

Supplementary Material 2

Supplementary Material 3

Supplementary Material 4

Acknowledgements

We are grateful to Kazuko Kaneda, Takanori Kobayashi, Rumi Saika and the TMIC staff for their excellent technical assistance. We also thank Edanz (https://jp.edanz.com/ac) for editing a draft of this manuscript.

Author contributions

All authors contributed to the study conception and design. TM, TW, HK, and KS conceived the conception and design of the study. TU, TW, KA, SN, and MM provides data acquisition. TU, TM, TW, HK, YY, NM, TY, MT, YS, TT, MS, and SN contributed to data analysis and interpretation. TU, TM, and TW drafted the manuscript, and other authors critically contributed to the manuscript. KS supervised the conduct of this study. All authors read and approved the final manuscript.

Funding

This study was funded by the JSPS KAKENHI (grant number 22K07231).

Data availability

No datasets were generated or analysed during the current study.

Code availability

Not applicable.

Declarations

Ethics approval and consent to participate

All the animal experiments were performed in compliance with the guidelines of the Institute of Experimental Animal Sciences. The protocol was approved by the Animal Care and Use Committee of the Osaka University Graduate School of Medicine (approval number 03-026-004).

Consent for publication

Not applicable.

Competing interests

The authors declare no competing interests.

Author details

[1]Department of Breast and Endocrine Surgery, Osaka University Graduate School of Medicine, 2-2-E10 Yamada-oka, Suita, Osaka 565-0871, Japan
[2]Department of Nuclear Medicine and Tracer Kinetics, Osaka University Graduate School of Medicine, Osaka, Japan
[3]Department of Radiology, Osaka University Graduate School of Medicine, Osaka, Japan
[4]Department of Advanced Radioisotope Medicine, Institute for Radiation Sciences, Osaka University, Osaka, Japan
[5]Linqmed Inc., Chiba, Japan
[6]Department of Pharmacy, Osaka University Hospital, Osaka, Japan

Received: 14 August 2024 / Accepted: 3 February 2025
Published online: 07 March 2025

References

1. Veronesi U, Paganelli G, Viale G, Luini A, Zurrida S, Galimberti V, Intra M, Veronesi P, Maisonneuve P, Gatti G, et al. Sentinel-lymph-node biopsy as a staging procedure in breast cancer: update of a randomised controlled study. Lancet Oncol. 2006;7(12):983–90.
2. Ashikaga T, Krag DN, Land SR, Julian TB, Anderson SJ, Brown AM, Skelly JM, Harlow SP, Weaver DL, Mamounas EP, et al. Morbidity results from the NSABP B-32 trial comparing Sentinel Lymph Node Dissection Versus Axillary Dissection. J Surg Oncol. 2010;102(2):111–8.
3. Liang X, Yu J, Wen B, Xie J, Cai Q, Yang Q. MRI and FDG-PET/CT based assessment of axillary lymph node metastasis in early breast cancer: a meta-analysis. Clin Radiol. 2017;72(4):295–301.
4. Mainiero MB, Cinelli CM, Koelliker SL, Graves TA, Chung MA. Axillary Ultrasound and Fine-Needle aspiration in the preoperative evaluation of the breast Cancer patient: an Algorithm based on Tumor size and Lymph Node Appearance. Am J Roentgenol. 2010;195(5):1261–7.
5. Han S, Choi J. Impact of ^{18}F-FDG PET, PET/CT, and PET/MRI on staging and management as an initial staging modality in breast Cancer a systematic review and Meta-analysis. Clin Nucl Med. 2021;46(4):271–82.
6. Kim T, Giuliano AE, Lyman GH. Lymphatic mapping and sentinel lymph node biopsy in early-stage breast carcinoma - A metaanalysis. Cancer. 2006;106(1):4–16.
7. Wei WJ, Rosenkrans ZT, Liu JJ, Huang G, Luo QY, Cai WB. ImmunoPET: Concept, Design, and applications. Chem Rev. 2020;120(8):3787–851.
8. Kurihara H, Hamada A, Yoshida M, Shimma S, Hashimoto J, Yonemori K, Tani H, Miyakita Y, Kanayama Y, Wada Y et al.: ^{64}Cu-DOTA-trastuzumab PET imaging and HER2 specificity of brain metastases in HER2-positive breast cancer patients. Ejnmmi Res 2015, 5.

9. Bai J, Qiu S, Zhang G. Molecular and functional imaging in cancer-targeted therapy: current applications and future directions. SIGNAL Transduct Target THERAPY 2023, 8(1).
10. Ulaner G, Mankoff D, Clark A, Fowler A, Linden H, Peterson L, Dehdashti F, Kurland B, Mortimer J, Mouabbi J, et al. Summary: Appropriate Use Criteria for Estrogen receptor-targeted PET imaging with 16α-^{18}F-Fluoro-17β-Fluoroestradiol. J Nucl Med. 2023;64(3):351–4.
11. Kurland B, Wiggins J, Coche A, Fontan C, Bouvet Y, Webner P, Divgi C, Linden H. Whole-body characterization of estrogen receptor status in metastatic breast Cancer with 16α-18F-Fluoro-17β-Estradiol Positron Emission Tomography: Meta-Analysis and recommendations for Integration into clinical applications. ONCOLOGIST. 2020;25(10):835–44.
12. Masuda H, Zhang DW, Bartholomeusz C, Doihara H, Hortobagyi GN, Ueno NT. Role of epidermal growth factor receptor in breast cancer. Breast Cancer Res Treat. 2012;136(2):331–45.
13. Cervantes A, Adam R, Roselló S, Arnold D, Normanno N, Taïeb J, Seligmann J, De Baere T, Osterlund P, Yoshino T, et al. Metastatic colorectal cancer: ESMO Clinical Practice Guideline for diagnosis, treatment and follow-up. Ann Oncol. 2023;34(1):10–32.
14. Machiels J, Leemans C, Golusinski W, Grau C, Licitra L, Gregoire, Board EE, Comm EG, Board EE. Squamous cell carcinoma of the oral cavity, larynx, oropharynx and hypopharynx: EHNS-ESMO-ESTRO Clinical Practice guidelines for diagnosis, treatment and follow-up. Ann Oncol. 2020;31(11):1462–75.
15. Bradley J, Paulus R, Komaki R, Masters G, Blumenschein G, Schild S, Bogart J, Hu C, Forster K, Magliocco A, et al. Standard-dose versus high-dose conformal radiotherapy with concurrent and consolidation carboplatin plus paclitaxel with or without cetuximab for patients with stage IIIA or IIIB non-small-cell lung cancer (RTOG 0617): a randomised, two-by-two factorial phase 3 study. LANCET Oncol. 2015;16(2):187–99.
16. Baselga J, Gómez P, Greil R, Braga S, Climent MA, Wardley AM, Kaufman B, Stemmer SM, Pêgo A, Chan A, et al. Randomized Phase II study of the anti-epidermal growth factor receptor monoclonal antibody Cetuximab with Cisplatin Versus Cisplatin alone in patients with metastatic triple-negative breast Cancer. J Clin Oncol. 2013;31(20):2586–.
17. Yoshii Y, Yoneda M, Ikawa M, Furukawa T, Kiyono Y, Mori T, Yoshii H, Oyama N, Okazawa H, Saga T, et al. Radio labeled Cu-ATSM as a novel indicator of overreduced intracellular state due to mitochondrial dysfunction: studies with mitochondrial DNA-less ρ^0 cells and cybnds carrying MELAS mitochondnal DNA mutation. Nucl Med Biol. 2012;39(2):177–85.
18. Yoshii Y, Yoshimoto M, Matsumoto H, Tashima H, Iwao Y, Takuwa H, Yoshida E, Wakizaka H, Yamaya T, Zhang MR, et al. Integrated treatment using intraperitoneal radioimmunotherapy and positron emission tomography-guided surgery with ^{64}Cu-labeled cetuximab to treat early- and late-phase peritoneal dissemination in human gastrointestinal cancer xenografts. Oncotarget. 2018;9(48):28935–50.
19. Watabe T, Kabayama K, Naka S, Yamamoto R, Kaneda K, Serada S, Ooe K, Toyoshima A, Wang Y, Haba H et al. Immuno-PET and targeted α-Therapy using anti-glypican-1 antibody labeled with ^{89}Zr or ^{211}At: a Theranostic Approach for pancreatic ductal adenocarcinoma. J Nucl Med 2023.
20. Kanda Y. Investigation of the freely available easy-to-use software 'EZR' for medical statistics. Bone Marrow Transplant. 2013;48(3):452–8.
21. Gradishar WJ, Moran MS, Abraham J, Abramson V, Aft R, Agnese D, Allison KH, Anderson B, Burstein HJ, Chew H. NCCN Guidelines® insights: breast Cancer, Version 4.2023: featured updates to the NCCN guidelines. J Natl Compr Canc Netw. 2023;21(6):594–608.
22. Lobo ED, Hansen RJ, Balthasar JP. Antibody pharmacokinetics and pharmacodynamics. J Pharm Sci. 2004;93(11):2645–68.
23. Zhou J, Ji Q, Li Q. Resistance to anti-EGFR therapies in metastatic colorectal cancer: underlying mechanisms and reversal strategies. J Exp Clin Cancer Res. 2021;40(1):328.
24. Ding F, Huang C, Liang CY, Wang C, Liu JJ, Tang DW. ^{68}Ga-FAPI-04 vs.^{18}F-FDG in a longitudinal preclinical PET imaging of metastatic breast cancer. Eur J Nucl Med Mol Imaging. 2021;49(1):290–300.
25. Hsu JL, Hung MC. The role of HER2, EGFR, and other receptor tyrosine kinases in breast cancer. Cancer Metastasis Rev. 2016;35(4):575–88.

Publisher's note